Global mapping of iron and titanium oxides in the lunar megaregolith and subsurface.

By *N. W Jackson [1] and B. D. Carter [1.]

[1] Department of Biological and Physical Sciences, University of Southern Queensland

Toowoomba, Australia 4350

* Contact person, **email** jackson_noel@uqconnect.net,

Abstract

This paper reports mapping results obtained by remote sensing analysis of Iron and Titanium oxides in the megaregolith under the lunar Highlands regolith and in the subsurface under the Mare and South Pole Aitken basin regolith. FeO and TiO_2 images were mosaicked from data extracted from the 1994 *Clementine* lunar orbiter mission from 60^0 N to 60^0 S, using the Lucey et al. technique (2000). These images then used to study the ejecta blanket for each of 2059 craters analysed using ISIS software (US Geological Survey). Average weight percentage values for each crater ejecta blanket were interpolated to derive underlying global Province Maps for FeO and TiO_2. The Moon was divided into five (5) provinces as a balance of the needs of analysis requirements and simplicity. Division of global TiO_2 weight percentages in the megaregolith /subsurface five provinces was matching the observed distribution of that at the surface. In contrast, division of lunar FeO into 5 Provinces reveals unexpectedly elevated iron concentrations (3.8 to 6.4%) in some areas of the Highland megaregolith. This Province of elevated iron oxide is termed “Highland II”.

Keywords

Moon, Clementine, mapping, crater, ejecta, megaregolith, subsurface.

INTRODUCTION

The Lunar Megaregolith and Subsurface

The Moon's surface regolith has been well studied using ground-based imaging and spectroscopy, lunar orbiter mapping, and sample return missions. In addition, at depth, the lunar bedrock rock type is indicated in the central peaks of craters over 50 km diameter, according to a spectroscopic analysis of *Clementine* data (Tompkins and Pieters, 1999).

In contrast however, the material between the regolith and bedrock has not been well mapped, especially on a systematic, global scale. This material between the regolith and bedrock is called the "megaregolith" by Hartmann (1973) who first coined the term ("mega-regolith"), stating that the lunar "megaregolith" is a major portion of the upper crust. Defined by Hartmann et al., 1986, as a "product of the cataclysm …. at least a few kilometres deep….". Since the term "megaregolith" is technically restricted to material beneath the anorthositic Highlands regolith, it is not suitable for material underlaying the regolith of maria and the South Pole Aitken basin. Therefore the term "subsurface" is substituted for "megaregolith" in non-Highland areas (see Appendix 1 for glossary). The work of Hartmann 1973 suggests that the crust broadly consists of the uppermost level consists of the regolith layer of up to a few metres in thickness, below that is a megaregolith of up to several kilometres in thickness, in Highland regions, overlying the bedrock. In mapping Fe0 and $Ti0_2$ weight percentage, five divisions were chosen as the optimum number to provide useful analysis.

This paper reports the final results of a global mapping study of Iron and Titanium oxides in the megaregolith under the lunar Highlands and in the subsurface under the Mare and South Pole Aitken basin as derived from crater ejecta.

The lunar megaregolith and subsurface contains keys to understanding the Moon's crustal history and development. Knowledge of this material is fundamental to our understanding of the evolution of the lunar crust and its impact history.

METHODOLOGY

Megaregolith Composition Characterisation

Crater ejecta like "drill-cores" (Spudis and Davis, 1986; Jackson, 2001) can be used to characterise the composition of the megaregolith/subsurface. Croft (1980), Grieve (1981) and later workers showed that for simple craters the effective depth of excavation is about ten percent of the diameter. Therefore, simple craters with diameters of approximately 5 to 50 km provide sample depths[1] of approximately 0.5 to 5 kilometres.

This approach, when coupled with the 1994 Clementine lunar orbiter mission (Nozette et al., 1994) and crater ejecta observations, provides an excellent method to sample the megaregolith and determine its FeO and TiO_2 content.

The 2059 craters selected for this study cover a range of 60^0 N to 60^0 S latitude globally. This limitation in latitudes is because of the large angles of incidence and

[1] Craters with diameters smaller than 5 kilometres have not been selected, as they would have insufficient depth for study of the megaregolith. Craters of diameters of 35 to 50 kilometres form less than 2.6% of the total population. Therefore complex craters do not significantly bias this study.

emergence of light at the lunar surface relative to the spacecraft's instruments and the Sun's illumination towards polar latitudes makes elemental mapping from Clementine images unreliable. From mosaicked multispectral images of Clementine data (Hapke, 1993; Nozette et al., 1994; Eliason et al., 1999), we used images with bands[2] centred on 415 nm, 750 nm and 950 nm (Nozette et al., 1994; Lucey et al., 2000), to make a three-layer mosaic from which to make iron (FeO) and titanium (TiO_2) images employing the technique of Lucey et al. (2000) and IDL software (www.ittvis.com accessed 2006). In essence, the Lucey et al. methods use Apollo lunar samples to provide a "ground-truth" (Table 1) for calibrating remote sensing data. In this work, the data were subsampled to 200 m/pixel. The subsampling averages the iron and titanium values, in this instance, over each 200 by 200 metre pixels. The smaller the pixel size of subsampling, the more technical problems arise, such as warping and registering the pixels of the image to the shape of a planetary surface. A larger pixel size is more forgiving to shaping images to a planetary surface. The 200meter pixels are most suitable for data extraction requirements for this global study.

For this project the iron and titanium global images were divided into 4 sectors, each 70 degrees in latitude and 90 degrees in longitude, for analysis using ISIS image software provided by the US Geological Survey, Flagstaff, Arizona USA.

For each bin of 10 degrees latitude by 10 degrees longitude, three to four craters were selected, based on pristine appearance (sharpness of the crater rim), and suitable diameter. Older craters of eroded or worn appearance or those with ejecta partly or totally covered or obscured by basalt flow material were excluded. Rare twinned craters were similarly not used, except where there were no others available. When twinned craters were analysed, only one of the twins was selected and the

[2] Drury (1990), "In remote sensing, a **band** is a range of wavelengths from which data are gathered by a recording device."

section of wall that was common was avoided, as the position of the ejecta blanket is not clear in these cases.

Asymmetric craters (e.g. elliptical in plan) were measured equal distances outward from the rim along both axes of symmetry; these craters make up a very small fraction (< 1 percent) of the population. The data were entered into a spreadsheet. Parameters used were: a sequential unique number for each crater (arbitrarily assigned numbers), name of crater (if known), (centre) latitude/ longitude, diameter of crater, iron (FeO) and titanium (TiO_2) weight percentage. The average weight percentage and standard deviation for FeO and TiO_2 were calculated from the data points in the ejecta around each crater. The province locations, Highland, Mare, and South Pole Aitken basin (SPA) were based on the terrane mapping of Jolliff et al. (2000) and were also recorded on the spreadsheet. The mapping of Jolliff et al (2000) was defined by distinct geomorphology, surface geochemistry derived from Clementine spectral data, and petrologic history divisions, not prejudiced by statistical clustering effects. This mapping is used as a reference for comparison and further study. Individually assigned numbers for each crater allows the use of Geographic Information System software such as ArcGIS 8.3 (www.esri.com accessed 2005) for mapping. Topographical maps (Weir, 1990; and Gillis, 2001) and the photographic atlas of Kosofsky and El-Baz (1970) were used for this study.

Using linked iron (FeO) and titanium (TiO_2) images in ISIS (US Geological Survey image processing software); 12 points were selected just outside the crater rim in the ejecta blanket for each crater. By use of a computer cursor and linked iron and titanium images, the points' position for each coordinate can be precisely identified.

The ISIS software provided weight percentage measurements for iron and titanium to one decimal place at each location. For each ejecta blanket, the consecutively placed points were taken initially from the 12.00 o'clock position and then visually spaced counter-clockwise. Occasionally, a point was taken further away, but less than one crater radius distance, so that the reading remained within the ejecta. The values were recorded for each ejecta blanket onto the spreadsheet and then an average and standard deviation value were calculated using the spreadsheet functions (see *Appendix 2 for data set, http://nla.gov.au/nla.arc-25194).

The data points for each crater were hand-selected and measured. This approach enabled the measurement process to take account of anomalies (such as minor breaks) in the crater rims, and ejecta blanket asymmetry. This was done to ensure that the recorded values were with in the ejecta blanket.

RESULTS AND DISCUSSION

Iron and Titanium Distribution

The data for individual craters were used to construct a global scale Iron Distribution Map (Figure 1) and Titanium Distribution Map (Figure 2) for the lunar megaregolith/ subsurface. Each dot in the maps represents an individual crater position, and an average of the weight percentage for twelve points in the crater ejecta for iron or titanium, respectively. In Table 2 of example crater ejecta, it can be noted from the

standard deviation for iron and titanium values that not all crater ejecta were homogenous in iron and titanium values.

As expected, since basalt by its nature contains significant amounts of iron, the data as shown in Figure 1 reveal the high concentrations of iron in the megaregolith of the basaltic maria. However, Figure 1 also reveals an area surrounding basins and on the lunar far side of highland megaregolith richer in iron than expected (Jackson et al., 2004; Spudis et al., 2004). In contrast, other highland megaregolith material has a lower FeO value, of between 0.0 and 3.7 percent (grey dots), which is expected for anorthosite or similar low-iron content material.

The surface of the highland region with the underlying megaregolith elevated iron is interpreted as being anorthositic (Jolliff et al., 2000; and other workers). This unit of highland megaregolith with higher than expected iron content shall be referred to as “Highland II”, and is found in areas that surround all maria and South Pole Aitken basin(see Figure 1). The range of these enhanced iron values (pink/ light shaded dots) in the highlands megaregolith is from 3.8 to 6.4 weight percent. Jolliff et al. (2000) refer to the surface over this area as “eastern basin terrane”. From the data set, mare iron (FeO) values range from 6.5 to 18.3 weight percent. These high values are as expected for basaltic areas since basalt is higher in iron than anorthositic highland areas (Heiken et al., 1991, pp. 121-181; and also Appendix 2 for data set, http://nla.gov.au/nla.arc-25194). The data set clearly reveals this. There appears to be a grading of intensities of iron weight percentage values in maria areas, and a trend of decreasing iron values from the centre of maria into the anorthosite.

In some parts of the South Pole Aitken (SPA) basin and its surrounding area, volcanism has occurred (Pieters et al., 2001). These areas exhibit higher iron content of mostly 9.8 to 13.3 percent, although a few points are between 13.7 to 18.3 percent,

as well as moderately higher titanium content from 1.1 to a maximum of 4.9 weight percent (Figure 2) in parts of the basin. Over the remainder of the South Pole Aitken basin, high iron values are observed. The higher iron content of South Pole Aitken basin megaregolith may not entirely be due to basalt flow, but instead due to the exposure of mafic lower crust (Lucey et al., 1998).

The Titanium Values Distribution Map (Figure 2) reveals the high levels of titanium in northern Oceanus Procellarum megaregolith (an average of 5.0 to a maximum of 11.1 weight percent) and neighbouring maria due to titanium-rich basalt flows. However there are no unexpected high values for titanium in localised areas of the highland region that coincide with the enhanced iron values surrounding the various maria. There appears to be no apparent common areal relationship between the iron and titanium values on a global scale, and only a partial agreement in the maria. In some small highly localised Highland areas, there are isolated, anomalous iron and titanium-rich readings (see Table 3).

Mare Moscoviense on the lunar farside has a titanium megaregolith value of up to 7.8 weight percent (see Figure 2) and coincides with high iron values that indicate a predominately titanium basalt source.

Around the vicinity of the South Pole Aitken basin there are higher titanium values of between 1.1 and 4.9 weight percent and these values are apparent in Figure 2. These values coincide with iron values in the 6.5 to 9.7 percent range and there are even a few points of iron values range from 9.7 to 13.6 percent. Just within the northern boundary of the South Pole Aitken basin, there are titanium values of between 1.0 percent and 2.5 percent (Apollo basin maria). There are higher iron values that coincide with these titanium values as a result of titanium-rich basalts flows (Pieters et al., 2001).

Outside, bordering part of the South Pole Aitken basin are other areas with isolated higher titanium readings (see Figure 2); however, these all coincide with higher iron values. Such results have been interpreted in terms of localised minor titanium-rich basalt flows. Overall, the surface and megaregolith signatures for titanium distribution are thus essentially the same.

New Lunar Megaregolith Province Maps

Two new Lunar Province Maps (Figures 3 and 4) were produced from the Iron and Titanium Distribution Maps (Figure 1, Iron (FeO); and Figure 2, Titanium (TiO_2)) in the megaregolith/subsurface. Kriging[3] (Davis, 1986, pp 383-405) is used to interpolate values between the data points and then project these values onto a global map between 60^0N and 60^0S in the "D North American 1927 GCS Assumed Geographic" mapping projection on a spherical form using ESRI ArcGIS 8.3 software (www.esri.com, accessed 2005). The different groups of values were contoured as polygons in a Geographic Information System. The Geographic Information System software is capable of dividing the data into any number of groups or classes to provide Provinces required for this study. Thus, an experiment was undertaken dividing the data into different numbers of groups or classes to determine the best results. The use of 5 groupings or classes (Provinces) was found to be the optimum to

[3] "Kriging is a concept of regionalised variable… as a naturally occurring property that has characteristics intermediate between a truly random variable and one that is completely deterministic." "The estimating procedure is called '*kriging*'.", Davis (1986). Essentially, kriging estimates the values between known data value points for various geological features, in this instance, iron (FeO) and titanium (TiO_2) for the purposes of mapping.

provide the detail and clarity for maps required. For comparison with an image map of the Moon see Appendix 3.

The Lunar Iron Province Map

The ArcGIS 8.3 software was directed, without bias, to divide the subsurface data derived from crater ejecta into 5 Lunar Iron (FeO) Provinces.

i) Lunar Highlands I - low iron content (0.0 to 3.7 %)

ii) Lunar Highlands II – low-medium iron content (3.8 to 6.4 %)

iii) Lunar Mare I or South Pole Aitken I – medium iron content (6.5 to 9.7 %)

iv) Lunar Mare II - South Pole Aitken II – medium-high iron content (9.8 to 13.6 %)

v) Lunar Mare III - South Pole Aitken III – high iron content (13.7 to 18.3 %)

The maria areas and South Pole Aitken basin have been allocated equivalent provinces for simplicity. This enables the iron-poor megaregolith of the Highland region to display the area of low Iron Province Highland I and low-medium Iron Province Highland II. The remaining provinces relate to the maria and South Pole Aitken basin and are labelled with increasing iron values, namely Iron Province Mare I/ South Pole Aitken I, Iron Province Mare II/ South Pole Aitken II, Iron Province Mare III/South Pole Aitken III.

With the exception of Highland II Province, the medium-high, high and very high iron provinces coincide with the maria and South Pole Aitken basin. The megaregolith under Mare Moscoviense and especially Orientale do not display the higher mare iron intensities in the megaregolith province maps, although several individual higher values may be seen in Figure 1. In contrast, the megaregolith of the

South Pole Aitken basin displays a complex signature of up to 13.6 percent iron values. A few isolated points in Figure 1 show an iron concentration of up to 18.1%; however, these are averaged out by the nearest neighbour kriging calculations used to produce the new Iron Province Map of Figure 3 for the megaregolith/ subsurface.

For ease of interpretation, the mapping scale for all maps produced for this paper is approximately 1:86,000,000 in both latitude and longitude. This scale was derived by using US Geological Survey 1:5,000,000 lunar maps (Weir 1990). The scale was calculated using the relationship that Scale equals Distance on the New Map at the equator in this instance divided by the Distance on the USGS Maps and multiplied by the USGS Map Scale. In the USGS maps, a Conical Mercator or Polar Mercator projection is used and the scale varies from an equatorial 1:6,036,000 scale (approximately) to one of 1:5,000,000 at latitudes 34 degrees N-S (Weir, 1990). To expedite interpretation of the maps produced in this study, a bar scale has been provided to estimate approximate distances.

The Lunar Titanium Province Map

The global lunar titanium (TiO_2) map is divided into 5 provinces through divisions into 5 classes of titanium weight percentage average values (see Figure 4). This procedure is consistent with the methodology used for iron (FeO).

The 5 Lunar Titanium (TiO_2) Provinces are listed below:

i) Titanium I - very low titanium (0.0 percent to1.0 percent)

ii) Titanium II - low titanium (1.1 percent to 2.5 percent)

iii) Titanium III – medium titanium (2.6 percent to 4.9 percent)

iv) Titanium IV – high titanium (5.0 percent to 7.8 percent)

v) Titanium V – very high titanium (7.9 percent to 11.1 percent)

Most maria seem to be represented (even if only in part) in the Titanium Province Map. However, the South Pole Aitken basin has only a weak signature (up to 2.5 percent), mostly on the northern margins of the basin, and with a distribution that only partly covers the area of the iron distribution. In these areas of mixed titanium and iron signatures, these would most likely indicate titanium-rich basalts. However, as no physical samples were obtained from the South Pole Aitken basin during the Apollo program, it is not possible to verify these data further with geochemical evidence. In addition, around the approximate centre of Orientale, there is an oval of Titanium Province II material.

Province Titanium I (0.0 percent to 1.0 percent) mostly covers the Highland and some western mare areas, whereas Province Titanium II (1.1 percent to 2.5 percent) covers maria areas at the lowest intensity. Province Titanium III (2.6 percent to 4.9 percent), Province Titanium IV (5.0 percent to 7.8 percent) and Province Titanium V (7.9 percent to 11.1 percent), as expected, all cover titanium-rich mare areas. The largest coverage and highest concentrations of titanium appear in a part of Oceanus Procellarum centred on approximately 15N, 55E. In Mare Tranquillitatis, two smaller anomalous areas of iron and titanium points of higher values can be easily seen in Figures 1 and 2.

In the final maps, interpolation (kriging) has averaged out isolated outlier values. This is particularly so for Mare Moscoviense and Orientale. In the new lunar megaregolith Titanium Province Map (Figure 4) a kriging calculation of “nearest neighbour” values has been used to interpolate the data and average out the two higher values for Mare Moscoviense and the three higher values for Orientale seen in Figure 2. The small number of data points available in these two areas provides the best available result at this time.

CONCLUSION

Global TiO_2 mapping of the megaregolith and subsurface has divided the Moon into provinces with the observed distribution matching that at the surface. In contrast, division of lunar FeO into provinces reveals unexpectedly elevated iron concentrations (3.8 to 6.4%) in some areas of the Highland megaregolith. A province of elevated iron oxide has been found and is termed “Highland II”.

Acknowledgements

The authors would like to acknowledge the helpful comments from the following in preparation of this paper: Dr Paul Spudis of John Hopkins University/ Applied Physics Laboratory Maryland USA; Professor Emeritus Stuart Ross Taylor and Dr Marc Norman of the Australian National University in Canberra Australia; Dr Clive Neal of Notre Dame University, Indiana, USA; and Professor Lionel Wilson of the University of Lancaster (UK).

References

BLEWETT D.T., LUCEY P.G. HAWKE B.R. & JOLLIFF B.L. 1997 Clementine images of the lunar sample return stations. Refinement of FeO and TiO_2 mapping techniques, *Journal of Geophysical Research*, 102(E), pp 16,319- 16,325.

CROFT S.K., 1980. Cratering flow field: Implications for the excavation and transient expansion stages of crater formation. *Proceedings of the 9th Lunar and Planetary Science Conference*, Houston Texas, USA. p. 2347.

DAVIS J.C., 1986. Statistical and Data Analysis in Geology, Publishers *Wiley and Son*. New York, pp.146-147 and Pages 383–405.

DRURY S.A., 1990. A Guide to Remote Sensing. *Oxford University Press,* Oxford UK, p 185.

ELIASON E.M., McEWEN A.S., ROBINSON E.M., LEE E.M., BECKET T., GADDIS L., WELLER L.A., ISBELL C.E., SHINAMAN J. R., DUXBURY T., & MALARET E., 1999. Digital image processing for a global multispectral map of the Moon from the Clementine UVVIS imaging instrument, *Proceedings of the 30th Lunar Planetary Science Conference*, Houston Texas, USA, Abstract 1933.

GRIEVE R.A.F., 1981. Impact Cratering, *Nature,* Volume 291. p. 16.

HAPKE B., 1993. Theory of Reflectance and Emittance Spectroscopy, *Cambridge University Press,* Cambridge, UK.

HARTMANN W.K., 1973. Ancient Lunar Mega-Regolith and Subsurface Structure, *Icarus, Academic Press Inc,* USA, Volume 18, Number 4. pp. 634-636.

HARTMANN W.K., PHILLIPS R.J., & TAYLOR, G.J. editors, 1986. Origin of the Moon, *Lunar and Planetary Institute*, Houston USA.

HEIKEN G.H., VANIMAN D.T., & FRENCH B.M., 1991. Lunar Sourcebook – a user's guide to the Moon, *Cambridge University Press*. Cambridge UK, New York, USA, Melbourne Australia.

JACKSON N.W., 2001. A Study of the Basalts of Northern Oceanus Procellarum using Clementine Lunar Orbiter data", *Proceedings of the 1st Australia Space Science Workshop CD-ROM*, National Space Society of Australia Conference, University of Sydney, Australia.

JACKSON N.W., SPUDIS P.D., & CARTER B.D., 2004. Preliminary Findings of a Study of the Lunar Global Megaregolith, *Proceedings of the 35th Lunar and Planetary Science Conference* Houston Texas USA, Abstract 1055.

JOLLIFF B.L., GILLIS J.J., HASKINS L.A., KOROTEV R.L., & WIECZOREK M.A., 2000. Major lunar crustal terranes: Surface expressions and crust-mantle origins, *Journal of Geophysical Research,* 105. pp. 4197-4216.

JOLLIFF B.L., 1999. Clementine UVVIS multispectral data and Apollo 17 landing site. What can we tell and how well?, *Journal of Geophysical Research* 104(E6), 14, pp123-14,148.

KOSOFSKY L. J. & EL-BAZ F., 1970. The Moon as viewed by Lunar Orbiter, *Office of Technology Utilizations, National Aeronautics and Space Administration* Washington DC USA.

LANGEVIN Y., & ARNOLD J.R., 1977. The evolution of the lunar regolith, *Annual Review Earth and Planetary Science,* 5. pp. 449-489.

LUCEY P.G., TAYLOR G.J., HAWKE B.R., & SPUDIS P.D., 1998. FeO and TiO_2 concentrations in the South Pole Aitken basin: Implications for Mantle Composition and basin formation", *Journal of Geophysical Research,* Vol. 103, E2. pp. 3701-3708.

LUCEY P.G., BLEWETT D., & JOLLIFF BL., 2000. Lunar Iron and Titanium abundance algorithms based on final processing of Clementine ultraviolet-visible images," *Journal of Geophysical Research,* Vol. 105, E8 pp. 20297-20306.

MCKAY D.S., FRULAND R.M., & HEIKEN G.H., 1974. Grainsize and evolution of lunar soils, *Proceedings of the 5th Lunar Science Conference*. pp. 887-906.

NOZETTE S., RUSTAN R., PLEASANCE L.P., HORAN D.M., REGEON P., SHOEMAKER E.M., SPUDIS P.D., ACTON C.H., BAKER D.N., BLAUMONT J.E., BURATTI B.J., CORSON M.P., DAVIES M.E., DUXBURY T.C., ELIASON

E.M., JOKOSKY B.M., KORDAS J.F., LEWIS I.T., LICHTENBERG C. L., LUCEY P.G., MALARET E., MASSEY M.A., RESNICK J.H., ROLLINS C.L., PARK H. S., MCEWEN A.S., PRIEST R.E., PIETERS C.M., REISSE R.A., ROBINSON M.S., SMITH D.E., SORENSON T.C., VORDER BREUGGE R.W., & ZUBER M.T., 1994. Clementine mission to the Moon: Scientific overview, *Science.* pp. 1835–1839.

PIETERS C.M., HEAD III J.W., GADDIS L., JOLLIFF B., & DUKE M., 2001. Rock types of the South Pole- Aitken basin and extent of basaltic volcanism, *Journal of Geophysical Research*, Vol.106, E11. pp. 28001-28022.

SPUDIS P.D. & DAVIS P.A., 1986. A chemical and petrological model of the lunar crust and implications for lunar crustal origin. *Proceedings of the 17th Lunar and Planetary Science Conference 1; Journal of Geophysical Research*, 91, B13. pp. E84-E90.

SPUDIS P.D., JACKSON N., BALOGA S., BUSSEY B., & GLAZE L., 2004. The Composition of the Lunar Megaregolith: some initial results from Global Mapping. *Proceedings of the 35th Lunar and Planetary Science Conference*, Houston Texas USA, Abstract 1512.

TOMPKINS S., & PIETERS C.M., 1999. Mineralogy of the Lunar Crust: Results from Clementine, *Meteoritics & Planetary Science*, 34. pp. 25-41.

WEIR D. (editor), 1992. “Atlas of the Moon”; 1:5,000,000 Topographic Series, The Lunar Near-side, L 5M 0/0 R, 1992, MAP I-2276 (Sheet 1 of 2, 1992 and Sheet 2 of

2, 1992)). Projection is Conical/ Polar Mercator, published by the USA Department of the Interior, *US Geological Survey for NASA.*

Table 1. Sampling Station Coordinates and Soil Compositions (from Lucey et al. 2000A).

Site	Latitude, deg	Longitude, deg E	Pixels averaged	FeO, wt %	TiO_2, wt %
Apollo 11	0.7254	23.4870	5 × 5	15.8	7.5
Apollo 12	-2.9890	336.6869	3 × 3	15.4	3.1
Apollo 14 - LM	-3.6726	342.6038	3× 3	10.5	1.73
Apollo 14 - Cone	*-3.6560*	*342.6459*	1	10.3	1.6
Apollo 15 – LM	26.1384	3.6744	1	15.0	1.9
Apollo 15 – S1	26.0339	3.6434	1	16.8	1.6
Apollo 15 – S2	26.0131	3.6256	1	11.5	1.3
Apollo 15 – S4	26.0355	3.7011	1	16.6	1.2
Apollo 15 – S6	25.9780	3.7179	1	12.1	1.5
Apollo 15 – S7	25.9900	3.7064	1	13.9	1.1
Apollo 15 – S8	26.1424	3.6700	1	15.2	1.7
Apollo 15 – S9	26.1376	3.6113	1	16.9	1.8
Apollo 15 – S9a	26.1376	3.6042	1	20.4	2.0
Apollo 16– LM	-8.9548	15.5105	1	5.6	0.6
Apollo 16 – S1	-8.9548	15.4620	1	5.4	0.6
Apollo 16 – S2	-8.9548	15.4797	1	5.5	0.6
Apollo 16 – S4	-9.0796	15.5090	1	4.6	0.5
Apollo 16 – S5	-9.0592	15.5149	1	5.9	0.7
Apollo 16 – S6	-9.0549	15.5002	1	6.0	0.7
Apollo 16 – S8	*-9.0433*	*15.4797*	1	5.4	0.6
Apollo 16 – S9	-9.0346	15.4914	1	5.7	0.6
Apollo 16 – S11	-8.8054	15.5134	1	4.2	0.4
Apollo 16 – S13	-8.8300	15.5222	1	4.8	0.5
Apollo 17 – LM	20.1922	30.7418	1	16.6	8.5
Apollo 17 – S1	20.1560	30.7530	1	17.8	9.6
Apollo 17 – S2	20.0985	30.4962	1	8.7	1.5
Apollo 17 – S3	20.1700	30.5341	1	8.7	1.8
Apollo 17 – S5	20.1858	30.6936	1	17.7	9.9
Apollo 17 – S6	20.289	30.7712	1	10.7	3.4
Apollo 17 – S7	20.2914	30.7843	1	11.6	3.9
Apollo 17 – S8	20.2804	30.8491	1	12.3	4.3
Apollo 17 – S9	20.2256	30.8024	1	15.4	6.4
Apollo 17 – LRV1	20.1761	30.6541	1	16.3	8.0
Apollo 17 – LRV2	20.1795	30.6165	1	13.4	4.4
Apollo 17 – LRV3	20.1829	30.5955	1	14.8	5.5
Apollo 17 – LRV4/S2a	*20.1075*	*30.5164*	1	8.5	1.3
Apollo 17 – LRV5	20.1846	30.5561	1	9.8	2.6
Apollo 17 – LRV6	20.1937	30.5648	1	10.3	2.6
Apollo 17 – LRV7	20.2156	30.6333	1	16.1	6.8
Apollo 17 – LRV8	20.2048	30.6621	1	15.7	6.6
Apollo 17 – LRV9	20.2332	30.7490	1	14.6	6.1
Apollo 17 – LRV10	20.2825	30.7545	1	11.2	3.7
Apollo 17 – LRV11	20.2764	30.841	1	12.7	4.5
Apollo 17 – LRV12	20.1977	30.7812	1	17.4	10.0
Luna 16	-0.7077	56.3701	5 × 3	16.7	3.3
Luna 20	3.5423	56.4446	5 × 4	7.5	0.5
Luna 24	12.7471	62.0407	6 × 6	19.6	1.0

References for composition: see Blewett et al.[1997, Table 1] and Jolliff [1999, Table 4].

Table 2 *Examples from study data set of Iron data variance in individual craters in Highland areas. "X" denotes belonging to this category*

Sample Data for Highland Standard Deviation of Analysis of Lunar Crater Ejecta.

Crater Number	Co-Latitude	Ordinates Longitude	Crater Diameter (km)	Av. Iron Weight %.	Av. Titanium Weight %.	Standard Dev. Iron	Standard Dev. Titanium	Highland
3	7.7	1.4	23.0	9.4	1.6	0.7	0.3	**X**
4	1.7	5.2	10.7	8.0	0.8	0.5	0.1	**X**
5	1.6	6.9	6.0	4.9	0.6	0.9	0.1	**X**
8	21.5	1.9	20.0	6.9	0.6	2.0	0.2	**X**
12	40.3	4.9	14.0	9.2	1.0	1.5	0.2	**X**
19	58.9	17.2	22.1	9.3	0.6	1.7	0.2	**X**
21	45.6	20.1	11.9	8.1	0.5	1.7	0.2	**X**
22	42.5	13.6	12.5	4.6	0.6	1.7	0.2	**X**
23	38.6	10.8	33.5	6.0	0.7	2.4	0.2	**X**
85	23.9	57.0	21.0	5.3	0.8	2.0	0.2	**X**
86	20.4	49.4	18.9	4.2	0.8	0.7	0.1	**X**
87	28.8	55.0	11.9	1.5	0.3	1.1	0.1	**X**
88	27.1	60.1	31.6	2.7	0.5	0.8	0.2	**X**
89	36.5	53.7	25.5	4.0	0.4	1.1	0.1	**X**
90	33.8	58.6	13.5	3.9	0.3	1.7	0.1	**X**
91	37.3	59.7	15.5	2.8	0.4	1.4	0.1	**X**
92	40.6	55.6	16.8	3.4	0.3	1.1	0.1	**X**
93	43.4	52.6	11.2	6.1	0.6	1.6	0.2	**X**
94	43.0	66.3	18.7	6.4	0.7	2.1	0.4	**X**
95	45.0	51.9	12.6	5.5	0.4	0.9	0.1	**X**
96	46.3	39.2	14.3	6.7	0.5	2.2	0.2	**X**
97	56.3	55.4	14.7	3.5	0.3	1.8	0.2	**X**
98	58.8	52.8	13.2	4.1	1.0	2.8	1.8	**X**
104	53.5	66.1	18.0	2.6	0.3	1.7	0.1	**X**
105	54.4	62.5	29.2	3.4	0.4	3.2	0.3	**X**
106	49.1	63.3	10.0	4.3	0.3	1.8	0.2	**X**
107	49.1	63.3	10.1	5.0	0.4	2.0	0.2	**X**
108	48.0	64.1	13.6	3.9	0.5	1.8	0.2	**X**
109	47.4	70.0	11.1	4.5	0.4	2.2	0.2	**X**

Table 3. *Crater Ejecta containing Anomalous Iron (FeO) and Titanium (TiO_2) Values.*

Crater Number	Latitude	Longitude	Iron Av Wt percent	Ti Av Wt percent	Notes (Terrane Type)
846	15.6	-96.2	10.9	3.0	Highland
1061	50.5	-24.4	10.3	2.3	Highland
1062	52.2	-29.9	9.5	1.2	Highland
1106	54.4	-4.6	11.2	0.6	Highland
1119	17.5	-3.3	10	1.4	Highland
1128	45.5	17.5	10.1	0.9	Highland
1189	-37.9	16.9	10.9	1.3	Highland
1276	-19.8	37.3	4.6	1.3	Highland / Mare border
1547	-44.7	116.2	10.4	1.1	Highland
1694	-38.4	157.7	11.1	1.1	Highland
1738	-43	161.5	12.4	1.4	Highland
1739	-49.6	161.6	12.4	1.2	Highland
1760	-46.7	172.2	10.2	0.8	Highland
1761	-44	177.8	11.8	1.0	Highland
1762	-40.2	171.7	10.2	1.1	Highland
1763	-32.7	174.1	12.4	1.7	Highland
1791	-26.4	-170.7	11.8	1.0	Highland
1792	-34.2	-177.5	11.4	1.2	Highland
1793	-31.1	-170.6	12.6	1.8	Highland
1794	-36.8	-172.3	11.9	1.4	Highland
1832	-29.8	-165	10.9	1.2	Highland
1833	-28.6	-167.8	11.4	1.5	Highland
1836	-25.7	-169.2	10.2	1.2	Highland
1891	-48.7	-142.3	13.1	0.9	Highland
1892	-44.3	-143.7	10.3	0.7	Highland
1895	-43.7	-147.8	10.1	1.0	Highland
1900	-30.5	-147.3	10.1	1.0	Highland near small Mare.
2185	-39	-50.8	8.1	1.7	Highland
2215	-44.1	-46.4	10.2	1.1	Highland / Mare
2247	-31.2	-35.3	8.4	1.4	Highland
2350	-10.5	-5.1	8.6	1.0	Highland / Mare

Appendix 1

Glossary of Terms.

Crater. A depression on the Moon's surface predominately caused by a body (eg a meteorite or asteroid) impacting the surface excavating material.

Ejecta. The material that is excavated to form a crater

Ejecta blanket. This is the material that has been excavated and deposited around a crater.

Regolith. Is the near-surface unconsolidated mass of debris that overlies the megaregolith and is though to vary in depth but to be less than a few tens of metres in thickness (McKay et al., 1974; Langevin and Arnold, 1977).

Megaregolith. The broken up, impact processed outer few kilometres of the lunar crust between the regolith and bedrock in Highland areas (Hartmann et al., 1986).

Subsurface. The material beneath the regolith in Mare areas.

Bedrock. The consolidated part of crust below the megaregolith.

Basin. A very large impact crater usually has a diameter of greater than 300 km across

Highland. Light toned heavily craters areas of the Moon that consist of anorthositic material

Mare. Dark toned areas of the Moon that consist of basaltic material

South Pole Aitken basin. An ancient large basin of the far side of the Moon covering from about 55^0 South to the lunar South Pole, not visible from Earth.

Appendix 2

***Prime megaregolith data set** spread sheet (see http://nla.gov.au/nla.arc-25194) used in this study with headings of:-

Crater Number, crater central Latitude, Longitude, diameter, 12 point for FeO and 12 point for TiO_2 weight percentage distribution in each crater ejecta blanket, FeO weight percentage average , TiO_2 weight percentage average, and one statistical deviation for FeO and TiO_2 for each crater and terrane type of Highland, Mare, South Pole Aitken basin. This data set consists of analysis of 2,355 craters; however only 2059 crater ejecta were used in this study as the remainder were at latitudes higher then 60^0N and 60^0S where the data were considered unreliable.

Appendix 3 Image Maps of the Moon

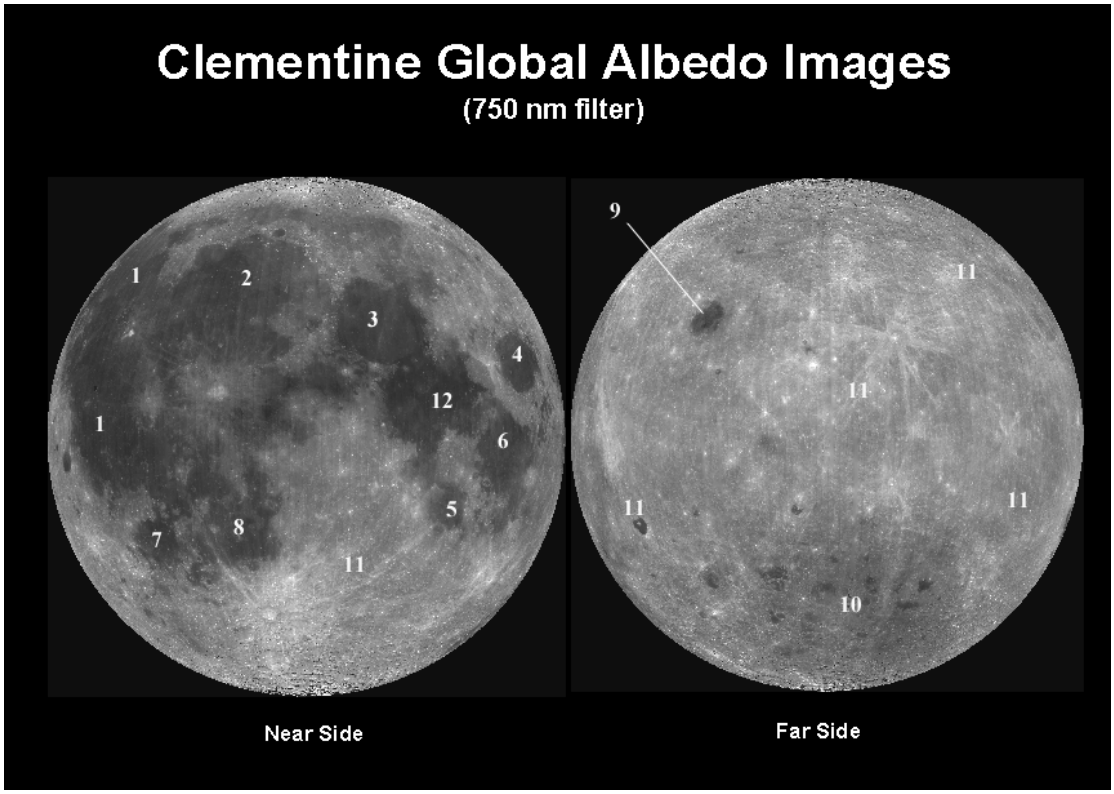

Figure B 1 *Map A. An Albedo image of the Moon using the 750nm mosaic from the Clementine of 1994 (Lunar and Planetary Institute Houston, Texas, USA. www.lpi.usra/clemen/albedo.gif*, accessed 2004*). The numbers represent the following features on the Moon's surface.*

1 = Oceanus Procellarum

2 = Mare Imbrium

3 = Mare Serenitatis

4 = Mare Crisium

5 = Mare Nectaris

6 = Mare Fecunditatis

7 = Mare Humorium

8 = Mare Nubium

9 = Mare Moscoviense

10 = South Pole Aitken basin

11 = Highland Terrane

12 = MareTranquilitatis

List of Figures.

Figure 4. *The Lunar Megaregolith/ Subsurface Titanium Province Map was derived by the interpolation of the Titanium Weight Percentage Distribution Map (Figure 2). The interpolation takes the values of surrounding pixels and derives a value for areas of no data using kriging (Davis, 1986). The scale is 1 degree = ~32 km, (Lunar and Planetary Institute, www.lpi.user.edu/clemen/ accessed 2004.)*

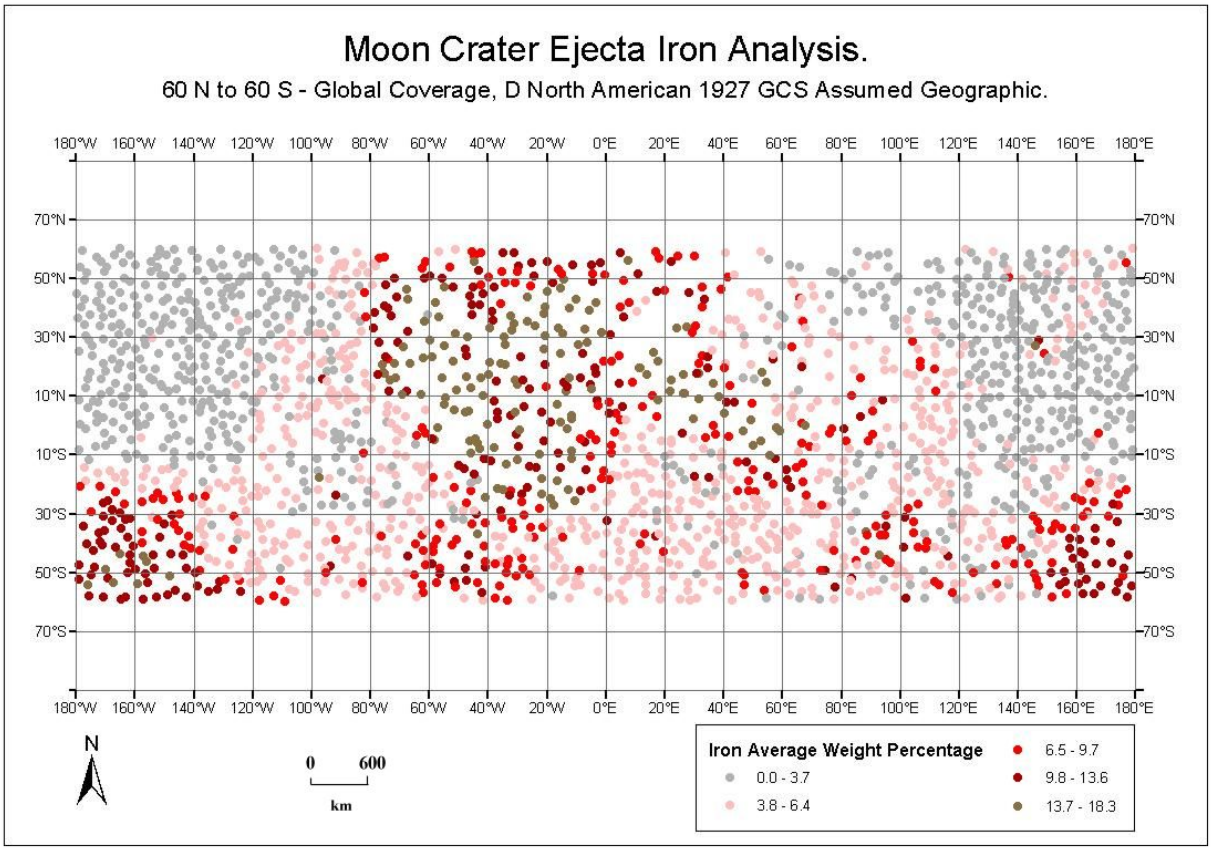
Moon Crater Ejecta Iron Analysis.
60 N to 60 S - Global Coverage, D North American 1927 GCS Assumed Geographic.
180°W 160°W 140°W 120°W 100°W 80°W 60°W 40°W 20°W 0°E 20°E 40°E 60°E 80°E 100°E 120°E 140°E 160°E 180°E
70°N
50°N
30°N
10°N
10°S
30°S
50°S
70°S
N
0 600
km
Iron Average Weight Percentage
0.0 - 3.7
3.8 - 6.4
6.5 - 9.7
9.8 - 13.6
13.7 - 18.3

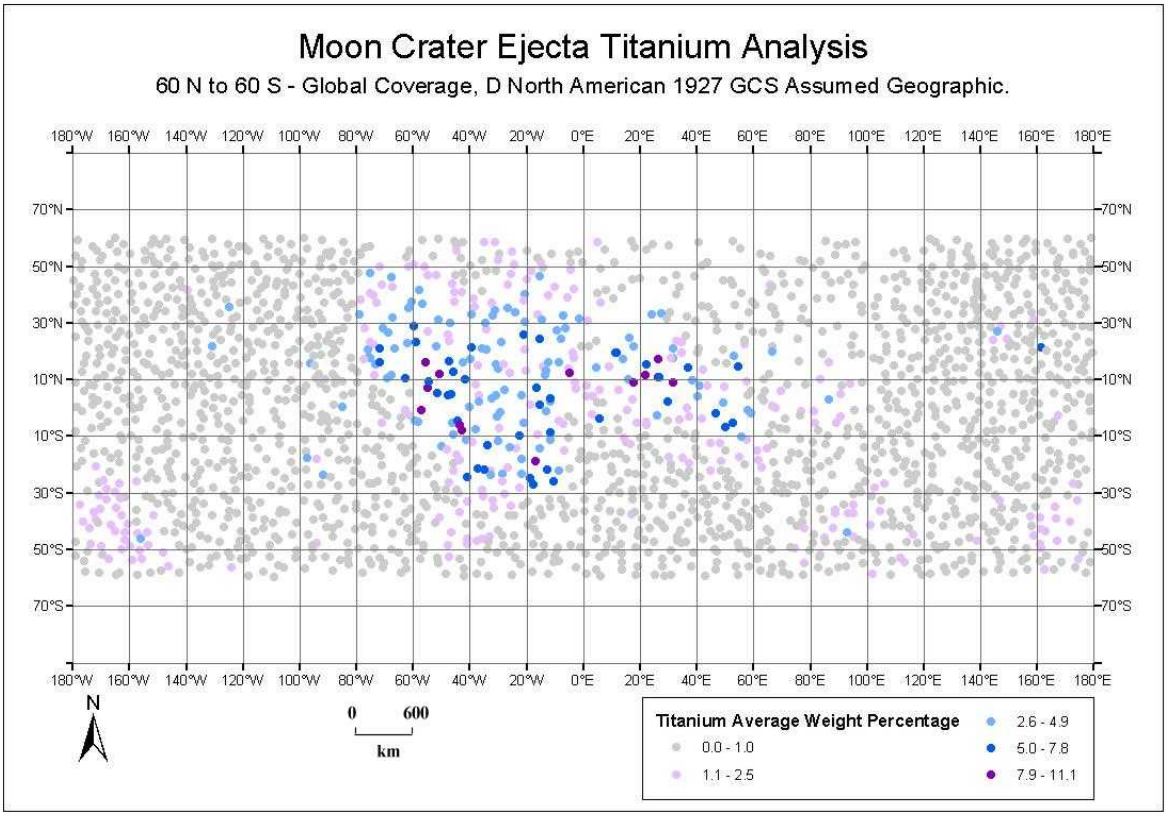
Moon Crater Ejecta Titanium Analysis
60 N to 60 S - Global Coverage, D North American 1927 GCS Assumed Geographic.
180°W 160°W 140°W 120°W 100°W 80°W 60°W 40°W 20°W 0°E 20°E 40°E 60°E 80°E 100°E 120°E 140°E 160°E 180°E
70°N
50°N
30°N
10°N
10°S
30°S
50°S
70°S
N
0 600
km
Titanium Average Weight Percentage
0.0 - 1.0
1.1 - 2.5
2.6 - 4.9
5.0 - 7.8
7.9 - 11.1

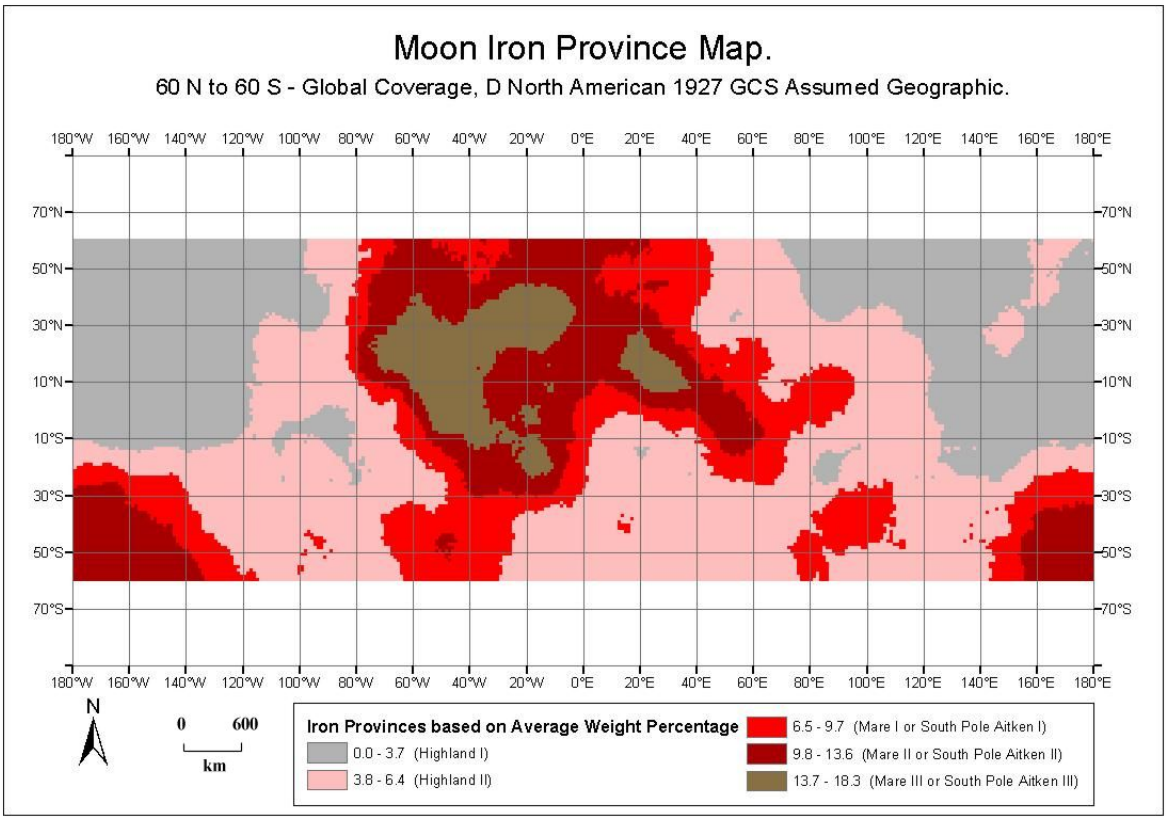
Moon Iron Province Map.
60 N to 60 S - Global Coverage, D North American 1927 GCS Assumed Geographic.
180°W 160°W 140°W 120°W 100°W 80°W 60°W 40°W 20°W 0°E 20°E 40°E 60°E 80°E 100°E 120°E 140°E 160°E 180°E
70°N 50°N 30°N 10°N 10°S 30°S 50°S 70°S
N
0 600
km
Iron Provinces based on Average Weight Percentage
0.0 - 3.7 (Highland I)
3.8 - 6.4 (Highland II)
6.5 - 9.7 (Mare I or South Pole Aitken I)
9.8 - 13.6 (Mare II or South Pole Aitken II)
13.7 - 18.3 (Mare III or South Pole Aitken III)

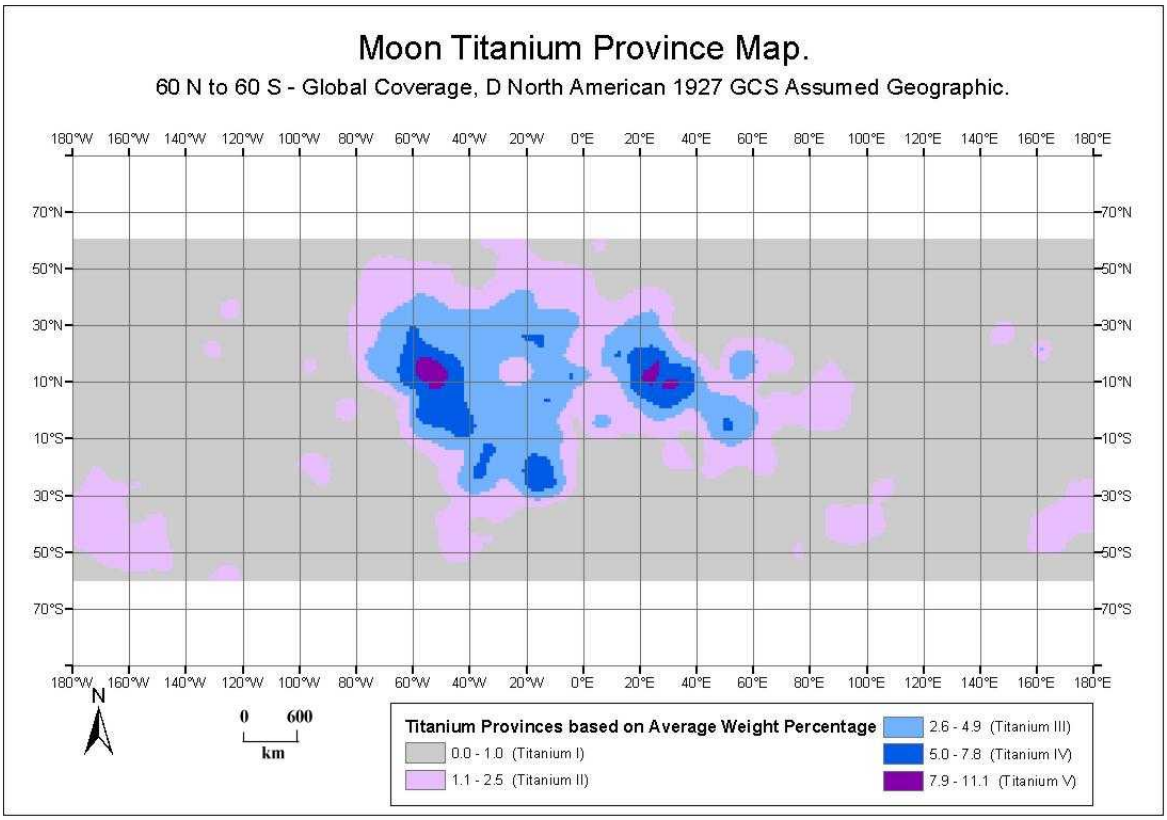
Moon Titanium Province Map.
60 N to 60 S - Global Coverage, D North American 1927 GCS Assumed Geographic.
180°W 160°W 140°W 120°W 100°W 80°W 60°W 40°W 20°W 0°E 20°E 40°E 60°E 80°E 100°E 120°E 140°E 160°E 180°E
70°N
50°N
30°N
10°N
10°S
30°S
50°S
70°S
N
0 600
km
Titanium Provinces based on Average Weight Percentage
0.0 - 1.0 (Titanium I)
1.1 - 2.5 (Titanium II)
2.6 - 4.9 (Titanium III)
5.0 - 7.8 (Titanium IV)
7.9 - 11.1 (Titanium V)